Available online at www.sciencedirect.com

ScienceDirect

www.elsevier.com/locate/jes

JES JOURNAL OF ENVIRONMENTAL SCIENCES

www.jesc.ac.cn

Pd-MnO_2 nanoparticles/TiO_2 nanotube arrays (NTAs) photo-electrodes photo-catalytic properties and their ability of degrading Rhodamine B under visible light

Mohamed Thabit[1], *Huiling Liu*[1,*], *Jian Zhang*[2], *Bing Wang*[1]

1. *State Key Laboratory of Urban Water Resource and Environment, School of Municipal and Environmental Engineering, Harbin Institute of Technology, Harbin 150090, China*
2. *School of Chemical Engineering, Northeast Electric Power University, Jilin 132012, China*

ARTICLE INFO

Article history:
Received 20 March 2017
Revised 6 June 2017
Accepted 26 June 2017
Available online 7 September 2017

Keywords:
Pd-MnO_2/TiO_2
Nanotubes
Photo electrode
Photo degradation
Rhodamine B
Photo-catalytic efficiency

ABSTRACT

Pd-MnO_2/TiO_2 nanotube arrays (NTAs) photo-electrodes were successfully fabricated *via* anodization and electro deposition subsequently; the obtained Pd-MnO_2/TiO_2 NTAs photo electrodes were analyzed by scanning electron microscopy (SEM), X-ray diffraction (XRD) and characterized accordingly. Moreover, the light harvesting and absorption properties were investigated *via* ultraviolet–visible diffuse reflectance spectrum (DRS); photo degradation efficiency was investigated *via* analyzing the photo catalytic degradation of Rhodamine B under visible illumination (xenon light). The performed analyses illustrated that Pd-MnO_2 codoped particles were successfully deposited onto the surface of the TiO_2 nanotube arrays; DRS results showed significant improvement in visible light absorption which was between 400 and 700 nm. Finally, the photo catalytic degradation efficiency results of the designated organic pollutant (Rhodamine B) illustrated a superior photocatalytic (PC) efficiency of approximately 95% compared to the bare TiO_2 NTAs, which only exhibited a photo catalytic degradation efficiency of approximately 61%, thus it indicated the significant enhancement of the light absorption properties of fabricated photo electrodes and their yield of .OH radicals.

Introduction

Since the beginning of this century the world suffered from a rapid increase of multiple types of environmental pollutants due to the increase of industrial hazardous materials emitted, poured, dumped or leaked into the ecosystem (Chen et al., 2013a; Cheng et al., 2013a; Yao et al., 2012) thus, with the onset of the environmental crisis, several researches were conducted to improve the technologies of pollutants' termination (Sun et al., 2013; Wei et al., 2013; Yu et al., 2014). One of those technologies which has shown great potential is the use of the photo catalytic properties of TiO_2 nanotube arrays (NTAs) to treat or terminate pollutants in wastewater and as a solar reactor application. It has been a remarkable candidate due to the low cost, non-toxicity and chemical stability of TiO_2, whilst its nanotube structure exhibits exceptional charge transport and excellent light harvesting properties. Therefore many efforts have been made to enhance its photo catalytic properties, which improves its application efficiency (Zhong et al., 2009; Momeni et al., 2015a; Momeni, 2015). However, TiO_2 can only be excited by ultraviolet light, which makes up only 3%–5% of the solar spectrum (Cheng et al., 2015; Chen et al., 2013b; Momeni and

* *Corresponding author. E-mail:* liuhl@hit.edu.cn (Huiling Liu).

https://doi.org/10.1016/j.jes.2017.06.042
1001-0742/

Ghayeb, 2015), therefore the use of narrower semiconductors has proven to be an effective technique, with high potential, to improve the visible light, photo catalytic performance of TiO_2. This is due to its ability to absorb more photons emitted from the light source. Moreover it has the ability to induce a higher photocatalytic (PC) efficiency due to the higher mobility and separation of the photo generation charge carrier (Momeni et al., 2015c, 2016a, 2016b; Cheng et al., 2013c; Cao et al., 2014). However, it was still required for there to be a number of semi-conductors, such as Pd, Ru, Cd, *etc.* (Momeni et al., 2015b; Momeni and Ghayeb, 2016a, 2016b), to enhance the catalytic performance of the Titanium dioxide nanotube arrays. These electrochemical capacitors with their high power density (Momeni et al., 2015c, 2016c; Momeni and Ghayeb, 2016c), long cycling life time, MnO_2 are a promising pseudocapacitive material with high theoretical specific capacitance. A study has shown that MnO_x can improve the absorption of visible illumination (Hu et al., 2016; Seong et al., 2015) and facilitate the electron–hole pairs to separate, because of their low charge transfer resistance and multitudinous defects (Zhou et al., 2016). MnO_x as a non-noble composite semiconductor catalyst: several studies on MnO_2 itself, as a catalyst, have shown results that were promising enough though they are not as significant as for noble catalysts (Sklar et al., 2005; Tian et al., 2012; Al-Sammarraie, 2014).

Literatures illustrated that manganese based catalysts are the most promising alternatives to metallic catalysts, due to their wide compounds variety. Among these compounds MnO_2, Mn_3O_4, Mn_5O_8 exhibited high activity. However, mixed oxides were found to be more active than pure MnO_x due to the presence of metal ions with different charges on the catalyst surface (Cheng et al., 2013b, 2013c).

Several studies on MnO_2 itself as catalyst have been performed, they reported remarkable capability of decomposing pollutants such as Acid Orange II under visible light (Sorge et al., 2015; Yang et al., 2014). However, it has been found that MnO_2 suffers from rapid capacity fade during cycling process, thus, some methods have been used to solve the problem such as developing nanostructured and nanotubes materials (Zhu et al., 2015; Wang et al., 2015) additionally, they have found that codoping MnO_2 with another nanomaterials improves structural and thermal stability (Seong et al., 2015). And the fabricated photoelectrodes become highly active for low temperature (Ettireddy et al., 2007; Jo and Lee, 2015).

Manganese dioxide (MnO_2) is not easily dissolved when bonding with other nanomaterials, thus, it does not pollute the aqueous medium during the administration of photocatalytic degradation processes (Okada et al., 2012).

Therefore, codoping MnO_2 with a noble semiconductor such Pd is a promising strategy as many researches have illustrated that the presence of a noble metal–semiconductor interface may induce effective charge separation to favor the subsequent photocatalysis (Momeni and Nazari, 2016).

There have been several studies of the synthesis of suitable semi-conductors on TiO_2 NTAs that have pursued this line of investigation. Following in the footsteps of these researches, we have sought to show in this study how Pd-MnO_2/TiO_2 NTAs photo electrodes have been fabricated successfully *via* anodization, followed by electro-deposition technique. The fabricated electrodes were tested and analyzed as shown in the following record of the experiment.

1. Materials and methods

1.1. Experimental materials and reagents

All chemicals used in this study are analytical grade and were employed without purification. Titanium sheets were purchased from Baoji and Baoye Titanium–Nickel Manufacturing Co., Ltd. Ammonium fluoride (NH_4F), ethylene glycol, acetone, absolute ethanol, and Rhodamine B were purchased from DINGSHENGXIN, China. Power supply (LPS305C-TC, BK PRECISION, USA) 0 to 30 V electric potential and 0 to 5 A electric current, magnetic agitators, 35 W xenon light source (D2S, Phillips, China), and 50 cm × 60 cm × 40 cm light isolation metal box were applied in this study.

1.2. Photo-electrode preparation

1.2.1. Titanium plate pretreatment

The size of the strip titanium sheet is 90 mm × 10 mm × 0.5 mm. The effective work area is 40 mm × 10 mm × 0.5 mm, the titanium foils were cleaned *via* immersion in a mixture of acetone and absolute ethanol and then in an Ultrasonic water bath for 30 min, the foils were left to dry for 1 hr at 80°C in vacuum oven, after being completely dried, the foils were immersed in a mixture of (HF: HNO_3: H_2O = 1:4:5 in volume) for 30 sec followed by a rinsing with deionized (DI) water then drying them in a vacuum oven for 4 hr at 70°C.

The polished titanium foils were anodized at a constant potential of 20 V in a mixture of water: ethylene glycol 1:9 containing 0.5 wt.% NH_4F aqueous solution at room temperature for 2 hr in a two-electrode configuration with a platinum cathode. After anodic oxidation, the samples were rinsed with deionized water and dried in air, the resulting amorphous TiO_2 NTs were annealed at 500°C for 2 hr with heating and cooling rates of 2°C/min in air to crystallize the tubes.

1.2.2. Preparation of Pd-MnO_2/TiO_2 NTAs photo-electrode

The electrolyte was an aqueous solution of 0.5 mol/L $Mn(CH_3COO)_2$ for preparation of MnO_2 deposition. Electrodeposition was carried out at room temperature, using a three-electrode potentiostatic control and direct current (DC) electrodeposition system with a saturated calomel electrode as reference electrode, a 1.0 cm × 1.0 cm platinum plate as a counter electrode and TiO_2 NTs substrate as working electrode. The electrolysis was carried out at 1.0 V for 2 hr. The foils were rinsed with DI water then annealed at 350°C for 2 hr. Afterwards the Pd nano-particles were electrodeposited onto the prepared MnO_2/TiO_2 electrode through the constant potentials in a three-cell configuration with MnO_2/NTAs electrode as cathode, platinum sheet as anode and SCE as reference electrode, which had been conducted at a constant potential of −0.8 V. in $PdCl_2$ solution (1 mmol/L) that contained 0.5 mol/L NaCl which served as the electrolyte. At the end the prepared photoelectrodes (Pd-MnO_2/TiO_2 NTAs) were rinsed by DI water, followed by drying at 70°C for 4 hr in a vacuum oven.

1.3. Photo-electrode characterization

In order to determine the characterization of the photoelectrode surface, several tests was performed such as scanning electron

microscopy (SEM) (QUANTA200F, Thermo Fisher Scientific, USA) to observe the distribution and dispersion of nano-particle on the electrode surface. X-ray diffraction (XRD) test (D/Max IIIB, Rigaku, Japan) was performed to detect the crystalline structure, grain size and the elementary composition. Reflectance spectroscopy (UV–Vis DRS) was recorded on a spectrophotometer (TU-1901, Xian Yima Optoelec Co., Ltd., China) equipped with an integrating sphere, in which $BaSO_4$ was used as the reflectance sample.

1.4. Evaluation of and photo catalysis (PC)

Photo catalytic activities of the samples were evaluated by using Rhodamine B as a model organic dye pollutant compound, the foils were immersed in a cylindrical quartz photo reactor contains 50 mL of Rhodamine B (5 mg/L), the TiO_2 NTAs electrode was placed vertically in the reactor then agitated with magnetic agitator, when the mixture reach the point of equilibrium the 35 W xenon light was switched on for 20, 40, 60, 80, 100 and 120 min, the sample were collected then measured at 552 nm using ultraviolet-vis (UV–vis) spectrophotometer (T60, PG Instruments Limited, China), the test was performed inside isolated metal box (light exposure chamber) with the dimension of 50 cm × 60 cm × 40 cm, these established equipment inside the isolated metal box (photo catalysis process chamber) are as shown in Fig. 1.

2. Results and discussion

2.1. SEM analysis

An SEM test was performed on the as prepared bare TiO_2 NTAs and the fabricated Pd-MnO_2 photoelectrode. Images shown in Fig. 2a represent the tubular structure of the nanotubes which exhibit the average inner diameter of 120 nm and 20 nm of wall thickness, while Fig. 2b illustrates the deposition of the Pd-MnO_2 particles onto the surface of the TiO_2 NTAs, the SEM image of Pd-MnO_2/TiO_2 NTAs shows the spots of Pd particles along with the rings of the deposited MnO_2 and can be easily observed to determine the existence of both Pd and MnO_2 nano particles. Thus, to confirm the elements deposited onto the fabricated nanotube arrays, further analysis has to be performed.

2.2. XRD and DRS analysis

The investigation into the crystalline structure of the fabricated Pd-MnO_2 was preformed *via* the XRD analysis patterns of the as-prepared bare samples. Noticeable, all observed XRD peaks can be indexed to the standard diffraction data of the corresponding (JCPDS No. 05–0681), anatase (JCPDS No. 21-1272), rutile (JCPDS No. 21-1276) and the Ti metal phase (JCPDS No. 44-1294), the X-ray diffraction pattern of the bare TiO_2 NTAs and Pd-MnO_2/TiO_2 NTAs composites film annealed at 350°C for 2 hr. The results shown in Fig.3 confirm the presence of the anatase phase of TiO_2 in the samples at (101), and the Ti diffraction peaks at (101), (102) and (103) were due to the Ti substrate,

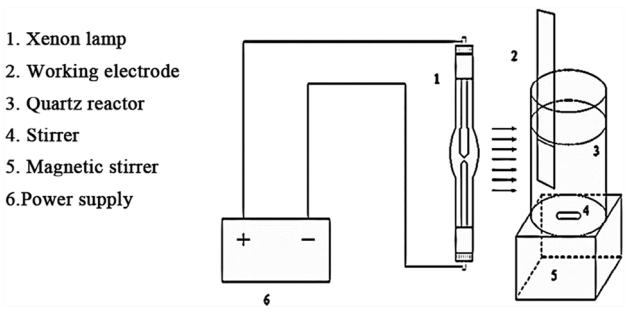

Fig. 1 – Diagram of equipment for photocatalytic oxidation.

However, the diffraction pattern of Pd-MnO_2/TiO_2 NTAs shows only the existence of traces of MnO_2 appeared at diffraction peaks (310), (211) and (301) while the diffraction peaks of Pd are not seen, which is likely due to the existence of Pd in particle form or a low composition therefore another analysis would be required to determine the existence of Pd on the surface of the fabricated photoelectrode.

In order to investigate the light absorption ability of the as prepared TiO_2 NTAs samples, UV–Vis diffuse reflectance spectra (DRS) analysis was performed on them. As shown in Fig. 4.

Both bare TiO_2 NTAs and Pd-MnO_2/TiO_2 samples exhibited a typical onset absorption edge at about 360 nm, corresponding to the electronic transition from O_2– anti-bonding orbital to the lowest empty orbital of Ti^{4+} (O2p → Ti3d) (Spadavecchia et al., 2010).

Nevertheless, compared with bare TiO_2 NTAs, the light absorbance edge of Pd-MnO_2/TiO_2 NTAs photoelectrode was significantly shifted to the visible region with the strongest peak located between 400 and 700 nm with a higher absorbance ratio, which could be attributed to the decoration of Pd-MnO_2, which is responsible for the improvement of visible light capability of Pd-MnO_2/TiO_2 NTAs. Furthermore, the band gap of TiO_2 NTAs could be calculated through the following Kubelka–Munk equation (Merabet et al., 2009)

$$(\alpha h\nu) = A\left(h\nu - E_g\right)^{n/2}$$

where ν, α, E_g, and A are the absorption coefficient, light frequency, band gap, and constant, while $h\nu$ is the photon energy and n is the semiconductor transition, respectively. Among them, n depends on the characteristics of the transition in a semiconductor, such as direct transition where $n = 1$ or indirect transition where $n = 4$. By estimating the band gap of TiO_2 NTAs and Pd-MnO_2/TiO_2 NTAs they were found to be 3.2 and 2.36 eV.

2.3. X-ray photoelectron spectroscopy (XPS) analysis

In order to clarify that the electrodeposited elements were successfully loaded onto the photoelectrode, XPS experiments were conducted to survey the surface concentrations of the atoms and to characterize the chemical species of the elements as shown in Fig. 5.

The manganese could be characterized *via* observing the Mn 2p peaks located between 640 and 660 eV, it has been demonstrated in the literature that the 2p3/2 binding energy of (MnO_2) is 642.5 ± 1 eV, the results obtained from the performed analysis have shown the Mn 2p peak at 642.13 eV, as shown in Fig. 5b, which indicates the existence of MnO_2 on the surface of the Photoelectrode.

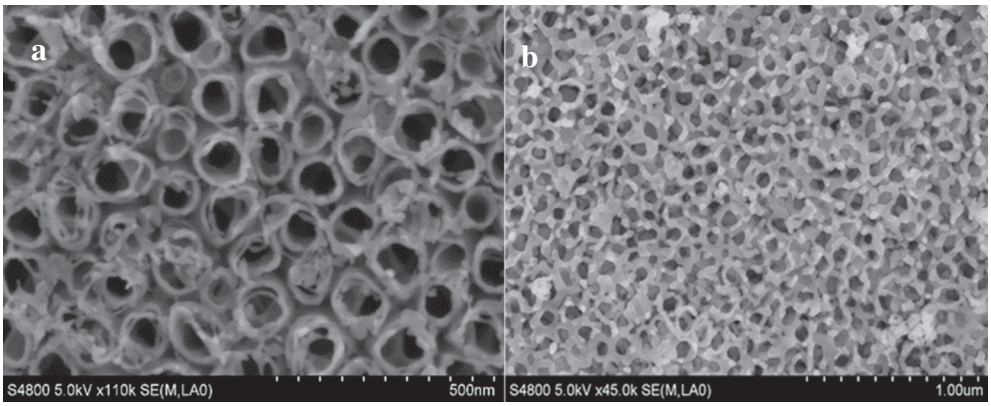

Fig. 2 – (a) Scanning electron microscopy images of bare titanium nanotubes arrays (NTAs) photo electrode and (b) Pd-MnO_2 decorated TiO_2 titanium nanotubes arrays.

The O 1s peaks comprised of two surface oxygen species. The O1s XPS spectra exhibited a main peak at about 530.33 eV, which was assigned to lattice oxygen from the metal oxides. The peak at 531.5–532.5 eV corresponded to the chemisorbed oxygen over the surface of the catalysts.

The Pd3d XPS is shown in Fig. 5d, the Pd3d spectrum consists of a high-energy peak (Pd3d3/2) at 340.93 eV and a low-energy peak (Pd3d5/2) at 335.73 eV. The spectrum can be deconvoluted into two doublets at 335.73 and 338.48 eV, corresponding to metallic Pd, which indicates that Pd was successfully loaded onto the surface of the Photoelectrode.

2.4. *Photocatalytic performance*

Photocatalytic activities of the samples were evaluated by using RhB as a model organic dye pollutant compound, the foils were immersed in a cylindrical quartz photo reactor containing 50 mL of RhB (5 mg/L), and Pd-MnO_2/TiO_2 NTAs electrode was placed vertically in the reactor then agitated with a magnetic agitator. When the mixture reached the point of equilibrium, the 35 W xenon light was switched on for 20, 40, 60, 80, 100 and 120 min, the samples were collected then measured at a 552 nm using UV–Vis spectrophotometer, the test was preformed inside an isolated metal box with the dimensions of 50 cm × 60 cm × 40 cm.

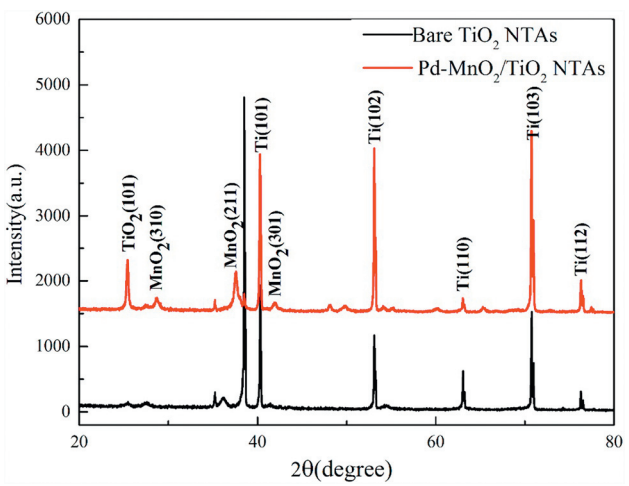

Fig. 3 – X-ray diffraction (XRD) patterns of the fabricated Pd-MnO_2/TiO_2, bare TiO_2 NTAs photoelectrodes.

The photocurrent response is an effective method to evaluate the photocatalytic performance of the fabricated Pd-MnO_2/TiO_2 NTAs photoelectrodes. The transient photocurrent response (PCR) was conducted to access the separation efficiency of photogenerated holes and electrons (h^+/e^-) pairs, under illumination, the photocurrent response generated promptly and remarkably increased, while the photocurrent response went down to null once the irradiation of light on the photoelectrode was stopped, suggesting the fabricated Pd-MnO_2/TiO_2 NTAs photoelectrodes were no longer produced a current. The transient photocurrent density of Pd-MnO_2/TiO_2 NTAs was significantly higher than bare TiO_2 NTAs, indicating a satisfactory separation efficiency of photogenerated charge carriers which is shown in Fig. 6.

Rhodamine B was often chosen as a representative pollutant to evaluate the photocatalytic performance of the as-synthesized catalysts. Thus, in this study, the degradation of RhB was used to evaluate the photocatalytic performances of the fabricated Pd-MnO_2/TiO_2 NTAs photoelectrodes. The degradation efficiencies (DE) of the collected samples were estimated *via* the following equation (Khataee et al., 2015)

$$DE = \frac{C_0 - C_t}{C_0} \times 100$$

where C_0 is initial concentration and C_t is concentration at processing time t. Compared with Pd/TiO_2 and MnO_2 efficiencies, the removal of direct photolysis or adsorption in the dark of RhB (<3%) was so low that it could be neglected.The photocatalytic performances of TiO_2 NTAs were greatly improved by decoration with Pd-MnO_2, which was supported by the DRS results, in addition, the results shown in Fig. 7 illustrated that codoping Pd-MnO_2 photoelectrodes has superior photocatalytic performance over singly doped Pd/TiO_2 and MnO_2, while Pd/TiO_2 showed higher performance than MnO_2/TiO_2. This is due to the high catalytic properties of noble elements, among which Pd is found.

The codoped Pd-MnO_2/TiO_2 TNAs exhibited highest photocatalytic performance for the degradation of Rhodamine B compared with that of the others, for which 97.6% of RhB

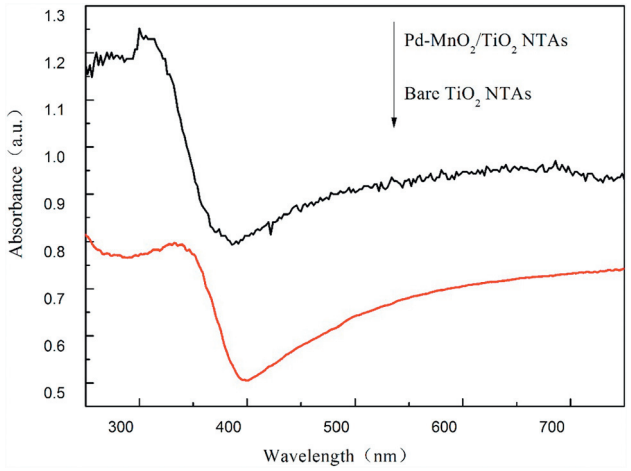

Fig. 4 – Ultraviolet–visible light absorption diffuse reflectance spectrum (DRS) patterns of Pd-MnO_2/TiO_2 NTAs and bare TiO_2 NTAs photoelectrodes. NTAs: TiO_2 nanotube arrays.

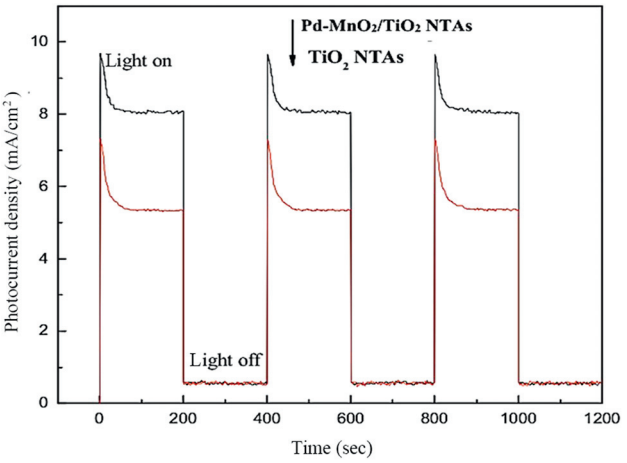

Fig. 6 – Photocurrent response of bare TiO_2 NTAs and Pd-MnO_2/TiO_2 NTAs photoelectrodes.

could be degraded within 120 min irradiation, which was attributed to the following two aspects.

(1) External potential facilitated the charge transfer and mobility, leading to a higher separation efficiency of photogenerated charge carriers, thereby inducing a higher photocatalytic degradation efficiency. (2) TiO_2 NTAs loaded with Pd-MnO_2 significantly improved the visible light absorption capacity, which could induce more photons to participate in the photocatalytic reaction, resulting in a higher photocatalytic efficiency.

The degradation rate of RhB fitted well with the pseudo-first-order kinetics function as shown in Fig. 8 according to the Langmuir–Hinshelwood (L–H) model within 120 min (Hoffmann et al., 1995)]

$$\ln\left(\frac{C}{C_0}\right) = -k_{app}t$$

where C is the concentration, C_0 is the initial concentration, and k_{app} is the constant of kinetic absorption and t is time.

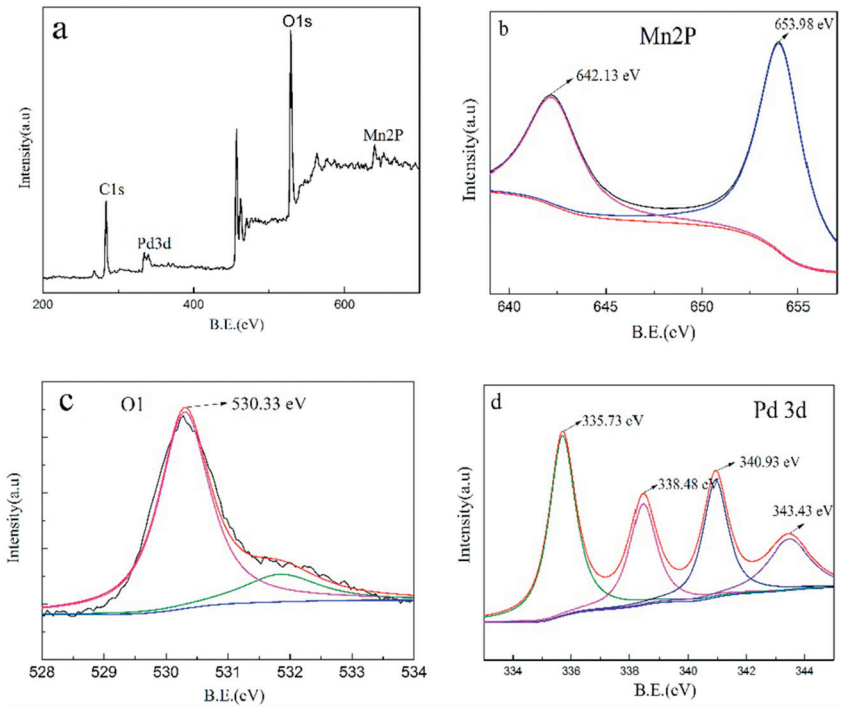

Fig. 5 – XPS (X-ray photoelectron spectroscopy) spectra diagram of (a) survey spectra, (b) Mn 2p spectrum, (c) O 1s spectrum and (d) Pd 3d spectrum. B.E.: binding energy.

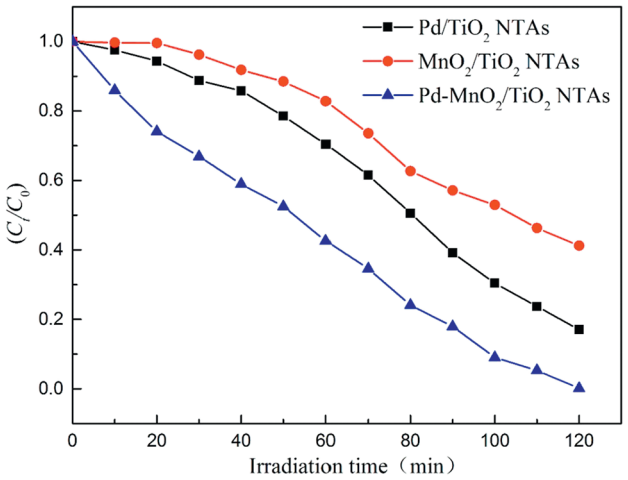

Fig. 7 – Rhodamine B degradation ratio during the illumination process, when C_0 is initial concentration and C_t is concentration at processing time t.

The fabricated Pd-MnO_2/TiO_2 photoelectrodes displayed the highest photocatalytic activity with a rate constant at 0.0259 min^{-1} under xenon light irradiation as shown in Table 1.

The photocatalytic stability of the fabricated photoelectrodes, which is important for their practical application, was tested to determine if they could be regenerated and salvaged. The concentration and stability of the solution of the designated organic pollutant (Rhodamine B) was kept in the dark and saved in black agar containers. Before administering the photodegradation process the mixture is agitated for 20 min inside an isolated metal box to reach a state of adsorption–desorption equilibrium. Afterwards the Pd-MnO_2 Photoelectrode is fixed in the photoreactor and illuminated for 2 hr. This process was repeated for seven successive-cycles. The results show that the catalyst exhibited catalytic performance without any significant deactivation, revealing its high stability after multiple reuses. There is no significant difference between the

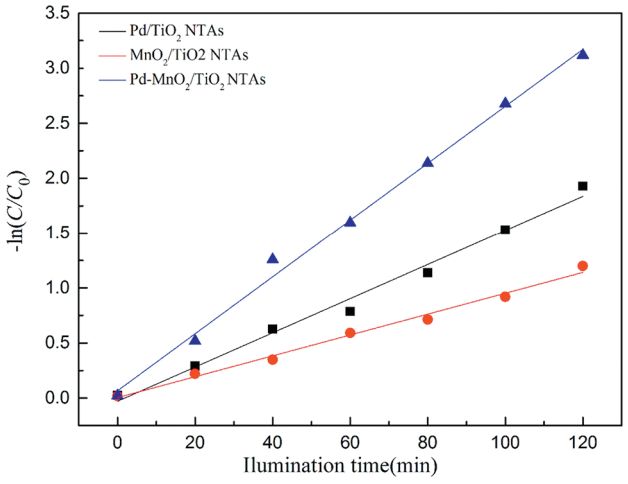

Fig. 8 – Photocatalytic evolution curves of RhB solution on Pd-MnO_2/TiO_2 NTAs, Pd/TiO_2 TNAs and MnO_2/TiO_2 TNAs photoelectrodes under 120 min of xenon light illumination. C is the concentration and C_0 is the initial concentration.

Table 1 – Photoelectrocatalytic degradation kinetics of Rhodamine B using Pd-MnO_2/TiO_2 NTAs, Pd/TiO_2 NTAs and MnO_2/TiO_2 NTAs photoelectrodes.

Samples	First order reaction kinetics equation	Apparent rate constants (k)	Correlation coefficient (R^2)
Pd-MnO_2/TiO_2	y = 0.0259x + 0.0663	0.0259	0.9954
MnO_2/TiO_2	y = 0.0155x – 0.029	0.0155	0.9882
Pd/TiO_2	y = 0.0095x+ 0.0045	0.0095	0.9909

NTAs: nanotubes arrays.

performance of the photoelectrode at the first cycle and the last one, and the degradation ratio deference is approximately – (2%–2.5%), the stability results are shown in Fig. 9.

3. Conclusions

Pd-MnO_2 nano particles were successfully codoped and loaded onto the surface of the fabricated TiO_2 nanotube photoelectrodes *via* the electrodeposition of MnO_2 in 3 electrodes cell, followed by annealing in a muffled furnace, afterwards, Pd particles were electrodeposited onto the obtained electrode *via* 3 electrodes electrodeposition cells. SEM results indicated the existence of the deposited particles onto the surface of the titanium dioxide nanotubes photoelectrodes, while the XRD analysis illustrated the existence of MnO_2, though it did not show Pd peaks, which could be due to Pd particle form or low composition. The existence of Pd and MnO_2 was determined by performing XPS analysis which showed that all targeted elements were successfully electrodeposited onto the surface of TiO_2 NTAs photoelecrodes. DRS analysis distinguished the difference of illumination absorption between bare TiO_2 and Pd-MnO_2/TiO_2, which had shown superior absorbance of illumination of UV light (λ < 400 nm) and intense visible light absorption ranging from 400 to 800 nm. Tthe results of Rhodamine B degradation have shown significant difference between Pd/TiO_2, MnO_2/TiO_2 and Pd-MnO_2/TiO_2 NTAs photoelectrodes, when Pd/TiO_2 having shown greater efficiency than MnO_2 photoelectrodes, while the

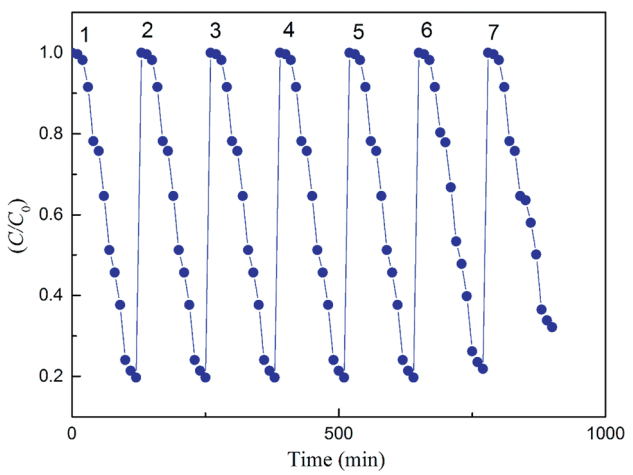

Fig. 9 – Photocatalyst stability test of prepared Pd-MnO_2 NTAs photoelectrodes.

combination of both materials expressed outstanding photocatalytic performance for the degradation of Rhodamine B because the decoration of Pd-MnO_2, which could provide the pathway for the transfer of the charge carrier. Furthermore, the contribution of series of active species scavengers demonstrated that •OH was the dominate species in the photocatalytic process. The remarkable stability shown by Pd-MnO_2/TiO_2 samples makes it a considerable candidates for the environmental applications of photocatalytic processes.

Acknowledgments

This work was supported by the National Natural Science Foundation of China (No. 51178138), the National Creative Research Groups of China (No. 51121062) and the State Key Laboratory of Urban Water Resources and Environment (No. 2010DX03).

REFERENCES

Al-Sammarraie, A.M.A., 2014. The role of anodizing potentials in making TiO_2 nanotubes in (ethylene glycol/NH 4 F /water) electrolyte. Arch. Appl. Sci. Res. 12 (5), 11–13.

Cao, G.-J., Bo, C., Wang, W.-Q., Tang, G.-Z., Feng, Y.-C., Wang, L.-P., 2014. Fabrication and photodegradation properties of TiO_2 nanotubes on porous Ti by anodization. Trans. Nonferrous Metals Soc. China 24 (8), 2581–2587.

Chen, Q., Liu, H., Xin, Y., Cheng, X., Zhang, J., Li, J., Wang, P., Li, H., 2013a. Controlled anodic growth of TiO_2 nanobelts and assessment of photoelectrochemical and photocatalytic properties. Electrochim. Acta 99, 152–160.

Chen, Q., Liu, H., Xin, Y., Cheng, X., 2013b. TiO_2 nanobelts–effect of calcination temperature on optical, photoelectrochemical and photocatalytic properties. Electrochim. Acta 111, 284–291.

Cheng, X., Liu, H., Chen, Q., Li, J., Wang, P., 2013a. Preparation and characterization of palladium nano-crystallite decorated TiO_2 nano-tubes photoelectrode and its enhanced photocatalytic efficiency for degradation of diclofenac. J. Hazard. Mater. 254, 141–148.

Cheng, X., Liu, H., Chen, Q., Li, J., Wang, P., 2013b. Construction of N, S codoped TiO_2 NCs decorated TiO_2 nano-tube array photoelectrode and its enhanced visible light photocatalytic mechanism. Electrochim. Acta 103, 134–142.

Cheng, X., Yu, X., Xing, Z., 2013c. Synthesis and characterization of C–N–S-tridoped TiO_2 nano-crystalline photocatalyst and its photocatalytic activity for degradation of Rhodamine B. J. Phys. Chem. Solids 74 (5), 684–690.

Cheng, X., Pan, G., Yu, X., 2015. Visible light responsive photoassisted electrocatalytic system based on CdS NCs decorated TiO_2 nano-tube photoanode and activated carbon containing cathode for wastewater treatment. Electrochim. Acta 156, 94–101.

Ettireddy, P.R., Ettireddy, N., Mamedov, S., Boolchand, P., Smirniotis, P.G., 2007. Surface characterization studies of TiO_2 supported manganese oxide catalysts for low temperature SCR of NO with NH_3. Appl. Catal. B. 76 (1–2), 123–134.

Hoffmann, M.R., Martin, S.T., Choi, W., Bahnemann, D.W., 1995. Environmental applications of semiconductor photocatalysis. Chem. Rev. 95 (1), 69–96.

Hu, J., Jiang, N., Li, J., Shang, K., Lu, N., Wu, Y., 2016. Degradation of benzene by bipolar pulsed series surface/packed-bed discharge reactor over MnO_2–TiO_2/zeolite catalyst. Chem. Eng. J. 293, 216–224.

Jo, S.H., Lee, H., 2015. Local structure and short-range ordering of MnO_2–$Ce_{(1-x)}Zr_xO_2$/TiO_2. Mater. Charact. 110, 102–108.

Khataee, A., Arefi-Oskoui, S., Fathinia, M., Esmaeili, A., Hanifehpour, Y., Joo, S.W., Hamnabard, N., 2015. Synthesis, characterization and photocatalytic properties of ER-doped PbSe nanoparticles as a visible light-activated photocatalyst. J. Mol. Catal. A Chem. 398, 255–267.

Merabet, S., Robert, D., Weber, J.V., Bouhelassa, M., Benkhanouche, S., 2009. Photocatalytic degradation of indole in UV/TiO_2: optimization and modelling using the response surface methodology (RSM). Environ. Chem. Lett. 7 (1), 45–49.

Momeni, M.M., 2015. Fabrication of copper decorated tungsten oxide–titanium oxide nanotubes by photochemical deposition technique and their photocatalytic application under visible light. Appl. Surf. Sci. 357, 160–166.

Momeni, M.M., Ghayeb, Y., 2015. Photoelectrochemical water splitting on chromium-doped titanium dioxide nanotube photoanodes prepared by single-step anodizing. J. Alloys Compd. 637, 393–400.

Momeni, M.M., Ghayeb, Y., 2016a. Fabrication, characterization and photocatalytic properties of au/TiO_2-WO_3 nanotubular composite synthesized by photo-assisted deposition and electrochemical anodizing methods. J. Mol. Catal. A Chem. 417, 107–115.

Momeni, M.M., Ghayeb, Y., 2016b. Fabrication, characterization and photoelectrochemical performance of chromium-sensitized titania nanotubes as efficient photoanodes for solar water splitting. J. Solid State Electrochem. 20 (3), 683–689.

Momeni, M.M., Ghayeb, Y., 2016c. Cobalt modified tungsten–titania nanotube composite photoanodes for photoelectrochemical solar water splitting. J. Mater. Sci. Mater. 27 (4), 3318–3327.

Momeni, M.M., Nazari, Z., 2016. Preparation of TiO_2 and WO_3–TiO_2 nanotubes decorated with PbO nanoparticles by chemical bath deposition process: a stable and efficient photo catalyst. Ceram. Int. 42 (7), 8691–8697.

Momeni, M.M., Ghayeb, Y., Davarzadeh, M., 2015a. Single-step electrochemical anodization for synthesis of hierarchical WO_3–TiO_2 nanotube arrays on titanium foil as a good photoanode for water splitting with visible light. J. Electroanal. Chem. 739, 149–155.

Momeni, M.M., Ghayeb, Y., Ghonchegi, Z., 2015b. Fabrication and characterization of copper doped TiO_2 nanotube arrays by in situ electrochemical method as efficient visible-light photocatalyst. Ceram. Int. 41 (7), 8735–8741.

Momeni, M.M., Hakimian, M., Kazempour, A., 2015c. In-situ manganese doping of TiO_2 nanostructures *via* single-step electrochemical anodizing of titanium in an electrolyte containing potassium permanganate: a good visible-light photocatalyst. Ceram. Int. 41 (10), 13692–13701.

Momeni, M.M., Hakimian, M., Kazempour, A., 2016a. Preparation and characterisation of manganese–TiO_2 nanocomposites for solar water splitting. Surf. Eng. 32 (7), 514–519.

Momeni, M.M., Mirhosseini, M., Chavoshi, M., 2016b. Growth and characterization of Ta_2O_5 nanorod and WTa_2O_5 nanowire films on the tantalum substrates by a facile one-step hydrothermal method. Ceram. Int. 42 (7), 9133–9138.

Momeni, M.M., Mirhosseini, M., Chavoshi, M., Hakimizade, A., 2016c. The effect of anodizing voltage on morphology and photocatalytic activity of tantalum oxide nanostructure. J. Mater. Sci. Mater. Electron. 27 (4), 1–7.

Okada, M., Tajima, K., Yamada, Y., Yoshimura, K., 2012. Self-organized formation of short TiO_2 nanotube arrays by complete anodization of Ti thin films. Phys. Procedia 32, 714–718.

Seong, M., Kim, S., Yoo, H., Choi, J., 2015. Doping of anodic nanotubular TiO_2 electrodes with MnO_2 for use as catalysts in water oxidation. Catal. Today 260, 135–139.

Sklar, G., Singh, H., Mahajan, Gorhe, V.D., Namjoshi, S., LaCombe, J., 2005. Nanoporous titanium oxide morphologies produced by

anodizing of titanium. MRS Proceedings. Cambridge Univ. Press, p. R1. 2.
Sorge, A.R., Turco, M., Pilone, G., Bagnasco, G., 2015. Decomposition of hydrogen peroxide on MnO_2/TiO_2 catalysts. J. Propuls. Power 20 (6), 1069–1075.
Spadavecchia, F., Cappelletti, G., Ardizzone, S., Bianchi, C.L., Cappelli, S., Oliva, C., Scardi, Leoni, P.M., Fermo, P., 2010. Solar photoactivity of nano-N-TiO_2 from tertiary amine: role of defects and paramagnetic species. Appl. Catal. B 96 (3), 314–322.
Sun, S., Chen, C., Sun, J., Peng, Q., Lü, K., Deng, K., 2013. Enhancement of catalytic degradation of rhodamine B under sunlight with Au loading TiO_2 nanotube arrays. Procedia Environ. Sci. 18, 620–624.
Tian, C.-Y., Zhao, W.-W., Wang, J., Xu, J.-J., Chen, H.-Y., 2012. Amplified quenching of electrochemiluminescence from CdS sensitized TiO_2 nanotubes by Cdte–carbon nanotube composite for detection of prostate protein antigen in serum. Analyst 137 (13), 3070–3075.
Wang, S., Li, Q., Pu, W., Wu, Y., Yang, M., 2015. MoO_3-MnO_2 intergrown nanoparticle composite prepared by one-step hydrothermal synthesis as anode for lithium ion batteries. J. Alloys Compd. 663 (01), 148–155.
Wei, B.X., Zhao, L., Wang, T.J., Gao, H., Wu, H.X., Jin, Y., 2013. Photo-stability of TiO_2 particles coated with several transition metal oxides and its measurement by rhodamine-B degradation. Adv. Powder Technol. 24 (3), 708–713.
Yang, H.T., Chen, B.M., Guo, Z.C., Liu, H.R., Zhang, Y.C., Huang, H., Rui-Dong, X.U., Ren-Chun, F.U., 2014. Effects of current density on preparation and performance of Al/conductive coating/a-PbO_2-CeO_2-TiO_2/β-PbO_2-MnO_2-WC-ZrO_2 composite electrode materials. Trans. Nonferrous Metals Soc. China 24 (10), 3394–3404.
Yao, Y., Li, K., Chen, S., Jia, J., Wang, Y., Wang, H., 2012. Decolorization of Rhodamine B in a thin-film photoelectrocatalytic (PEC) reactor with slant-placed TiO_2 nanotubes electrode. Chem. Eng. J. 187, 29–35.
Yu, X., Zhang, Y., Cheng, X., 2014. Preparation and photoelectrochemical performance of expanded graphite/TiO_2 composite. Electrochim. Acta 137, 668–675.
Zhong, H., Shaogui, Y., Yongming, J., Cheng, S., 2009. Microwave photocatalytic degradation of rhodamine B using TiO_2 supported on activated carbon: mechanism implication. J. Environ. Sci. 21 (2), 268–272.
Zhou, H., Zou, X., Zhang, Y., 2016. Fabrication of TiO_2 @MnO_2 nanotube arrays by pulsed electrodeposition and their application for high-performance supercapacitors. Electrochim. Acta 192, 259–267.
Zhu, Q., Hu, H., Li, G., Zhu, C., Yu, Y., 2015. TiO_2 nanotube arrays grafted with MnO_2 nanosheets as high-performance anode for lithium ion battery. Electrochim. Acta 156, 252–260.